Volume 264, Issues 1–2 15 December 2007 ISSN 0012-821X

ELSEVIER

EARTH & PLANETARY SCIENCE LETTERS

Available online at www.sciencedirect.com
ScienceDirect
Earth and Planetary Science Letters 264 (2007) 299–307
EPSL
www.elsevier.com/locate/epsl

Rapid mantle flow beneath the Tonga volcanic arc

James A. Conder *, Douglas A. Wiens

Department of Earth and Planetary Sciences, Washington University, St. Louis, MO, 63130, USA

Received 7 April 2007; received in revised form 8 August 2007; accepted 2 October 2007
Available online 14 October 2007
Editor: C.P. Jaupart

Abstract

Flow in the Earth's asthenospheric mantle is typically assumed to be driven by motions of the overlying and adjacent plates, suggesting flow rates comparable to plate velocities. However, arc-parallel shear-wave splitting and geochemical observations imply along-strike flow in the Lau basin, presenting a challenge to geodynamic models of plate-driven subduction systems as plate-driven flow models predict arc-perpendicular fast direction with simple (A-type) mineral texturing. Although B-type mineral texturing would result in the fast directions developing 90° relative to A-type and likely occurs in the forearc mantle, such texturing is unlikely in the asthenosphere wedge where higher temperatures and weak rheology likely prevail. By tracking mineral texturing development within geodynamic flow models patterned after the Tongan system in the Lau basin that include along-strike flow, we find that the observations are best explained by models including rapid along-arc flow within the subarc mantle. The effect of melt on the anisotropy does not appear to be a primary control, but needs to be investigated more fully. The best fit to the observations is a model with along-strike flow within a low-viscosity channel beneath the arc at a rate of nearly 50 cm/yr, several times the plate motion velocities.

Keywords: subduction; dynamics; seismic anisotropy

1. Introduction

Most conceptual and physical models of mantle flow at subduction zones in the literature presuppose 2-dimensional corner flow. However, a steadily increasing body of evidence has been accumulating over the last decade showing that many arcs have a significant component of along-strike flow in the mantle wedge beneath the arc. Evidence for along-strike flow beneath arcs comes from seismic anisotropy (Smith et al., 2001; Fischer et al., 1998) (Fig. 1), geochemical studies (Turner and Hawkesworth, 1998; Pearce and Stern, 2006; Leat et al., 2004) and, petrofabrics within an exhumed arc (Mehl et al., 2003).

In the Lau basin and elsewhere, seismic anisotropy measurements are widely cited and invoked for interpretation of along-arc flow as experimental works shows that seismically fast olivine *a*-axes tend to align in the direction of maximum shear (A-type mineral fabric) (Zhang and Karato, 1995).

Notably, the interpretation of seismic anisotropy is subject to exactly how the lattice-preferred orientation (LPO) of mantle minerals develops during flow which can be markedly different under different regimes of stress and/or water content (Jung and Karato, 2001;

* Corresponding author. Washington University, Campus Box 1169, One Brookings Dr St. Louis, MO, 63130, USA. Tel.: +1 314 935 7372; fax: +1 314 935 7361.
E-mail address: conder@seismo.wustl.edu (J.A. Conder).

0012-821X/$ - see front matter © 2007 Elsevier B.V. All rights reserved.
doi:10.1016/j.epsl.2007.10.014

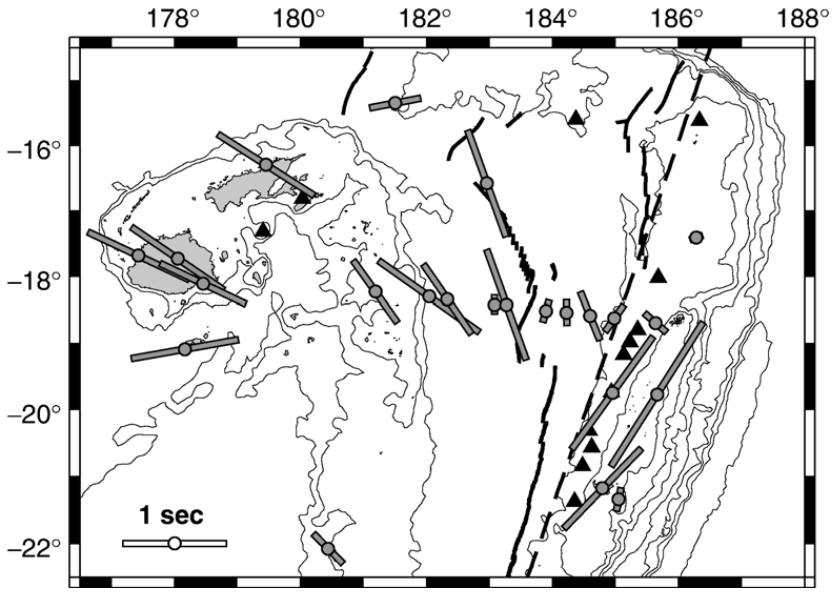

Fig. 1. Map of Lau basin. Thin lines are bathymetric contours at 1 km increments. Triangles denote active volcanoes. Circles show seismic stations (both OBS and island stations) used for splitting analysis of Smith et al. (2001). Vectors show stacked splitting directions for local S phases measured at each station. Dashed line delineates extracted bathymetry line for examination of dynamic topography along the arc. Open white vector is scale bar of 1 s.

Jung et al., 2006). For example, the development of B-type LPO is demonstrated in the Higashi-akaishi exhumed forearc in southwest Honshu (Mizukami et al., 2004). Unlike the forearc, the mantle asthenosphere has temperatures too high and viscosities too low to support the stresses necessary (>300 MPa) to be in the B-type LPO development regime (Kneller et al., 2005). At least locally, C-type fabrics are possible. Within the wedge, C-type fabric will likely develop where wedge water contents exceed ~1000 ppm H/Si (Jung et al., 2006) resulting in the fast axes normal to the shear plane. For vertically traveling rays, the polarization direction of the fast S-wave will be similar to A-type fabrics, but the splitting times should be considerably smaller. E-type fabrics may also be prevalent in the mantle wedge (Jung et al., 2006), but fast axis alignment is seismically indistinguishable from A-type development. For the purposes of this paper we focus on A-type fabric development and subsequent seismic anisotropy development with various flow patterns within the wedge mantle, with the caveat that fast polarization directions will be better constrained than splitting times due to the possibilities of C- and E-type fabrics being distributed within the wedge.

Independent evidence for along-arc flow from north to south is inferred in the Lau basin from Helium isotopes (Turner and Hawkesworth, 1998) and other stable elemental ratios Pearce and Stern, 2006. Elevated $^{3/4}$He isotope ratios extend only a few hundred kilometers into the basin, seemingly suggesting a slow influx of incoming asthenosphere. However, a small amount of melt extraction can quickly erase the $^{3/4}$He plume signature in the mantle (Pearce and Stern, 2006), and other tracers such as Nb/Yb, a measure of mantle fertility that is insensitive to the addition of subduction components, suggest that southward mantle flow has coursed the entire length of the sampled arc (Pearce and Stern, 2006). Mantle flow that has coursed the length of the arc implies a minimum rate of 20 cm/yr (~1000 m within 5 yr of opening, Taylor et al., 1996).

Along-strike flow of the wedge mantle may be imposed from lateral motion of the overriding plate (Hall et al., 2000; Honda and Yoshida, 2005) or from within the asthenosphere due to internal pressure gradients (Conder et al., 2002; Phipps Morgan and Smith, 1992; Yale and Phipps Morgan, 1998). Because GPS studies of the Tonga region show little lateral motion of the overriding plates (Bevis et al., 1995), we explore only the latter condition of internally driven asthenospheric flow. Along-arc flow likely arises from flow around the slab edge during rollback (Leat et al., 2004; Buttles and Olson, 1998) or by impingement of the Samoan plume at the northern end of the subduction system (Smith et al., 2001; Turner and Hawkesworth, 1998). Either of these mechanisms could support a long-lived mantle pressure gradient that drives flow along-strike. In this paper, we compare the observed shear-wave splitting results from local S phases (Smith et al.,

2001) (Fig. 1) to predictions of geodynamic models of mantle flow and associated texturing of the mantle within the asthenosphere of the Lau Basin to estimate the rate of mantle flow beneath the Tonga arc in the Lau basin necessary to explain the shear-wave splitting. The model that best fits the observed splitting calls for rapid, channeled flow within a low-viscosity upper corner of the wedge with peak velocity approaching 50 cm/yr, demonstrating that flow may be significantly faster than typical plate tectonic velocities.

2. Methods

To constrain the magnitude of plausible driving pressures in the Lau basin asthenosphere from either rollback or plume impingement, we check for possible dynamic topography along the extent of the arc by extracting a bathymetric line along the west side of the active volcanic chain from ETOPO2v2 (U.S. Department of Commerce, 2006) (Fig. 1). As bathymetric transects near the arc cannot reasonably avoid seamounts or other volcanic structures, our line is fairly noisy. Nevertheless, there is a discernible trend of deepening seafloor from north to south (Fig. 2). A simple, least-squares fit to the extracted bathymetric line results in a 0.8 m/km topographic gradient from south to north, although any slope from 0.4 to 1.2 m/km could reasonably fit the data. Nearby lines are similarly, if not more noisy, but all consistently exhibit similar trends with slopes deepening towards the south of at least 0.3 m/km along the arc.

Potentially, dynamic topography could be manifested in the free air gravity anomaly. However, because of the shallowness of the topographic gradient, the associated free air gravity anomaly would be a fraction of a mgal over this length and is therefore unfortunately much too small to be confirmed through the gravity signal. As there is no clear systematic along-arc mantle velocity variation indicative of a temperature gradient in tomographic results (Pillet et al., 1999), we assume that at least some of this bathymetric slope is supported by a dynamic pressure gradient rather than solely through some intrinsic north to south mantle density gradient. A gradient in crustal thickness could account for the topographic gradient, but at present, the data do not exist to demonstrate whether this is the case. Assuming no systematic along-arc variation in crustal thickness with a mantle-ocean density contrast of 2300 kg/m^3 and recognizing that dynamic pressures may be partially compensated by deflections on a deeper mantle density contrast (Phipps Morgan and Smith, 1992), a topographic slope of 0.8 m/km suggests a north to south pressure gradient upwards of 50 kPa/km within the arc mantle to support the dynamic topography and subsequently drive southward asthenospheric flow.

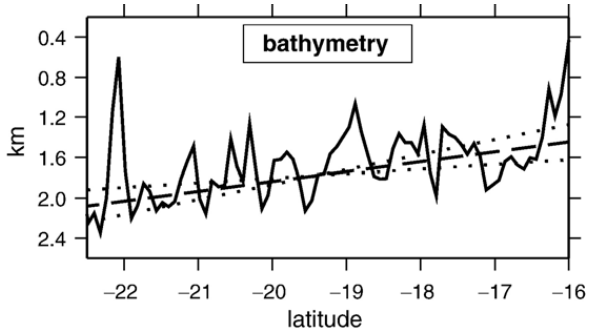

Fig. 2. Bathymetric transect for a line along the west side of the Tonga volcanic arc. Location marked in Fig. 1. Even with the rough topography including numerous seamounts, there is a clear slope from north to south possibly indicating dynamic pressure gradient within the arc asthenosphere that could drive asthenospheric flow along the arc. Best fitting slope is 0.8 m/km (dashed line) ±0.4 m/km (dotted lines), suggesting dynamic pressures upwards of several 10 s of kPa/km.

To investigate the required patterns and magnitude of along-strike flow in the Lau mantle wedge, we expand previous 2D, finite-element, variable-viscosity, flow modeling (Conder, 2005) to incorporate flow in the along-strike direction. To keep the models simple, we assume that along-strike flow develops with a pressure gradient parallel to the trench and that flow velocity does not vary in the along-strike direction. The flow model comprises 181×121 variably-spaced nodes on a 500×400 km grid, with grid resolution approaching 1 km at 40–50 km depth in the asthenospheric wedge (Conder, 2005). We kinematically subduct the slab at a 45° dip at a rate of 9 cm/yr to simulate Pacific motion relative to Fiji (Bevis et al., 1995). We ignore the back-arc spreading center as it is a secondary control on the flow field of interest and the 2.5D assumption would over-predict expected flow along the axis as pressures are uniform across the model. The viscosity structure depends on temperature, pressure, and strain-rate, assuming a stress exponent of 3 and activation volume and energy of 15×10^{-6} m^3/mol and 500 kJ/mol respectively in the dislocation regime and half of the activation values in the diffusion creep regime (Mei and Kohlstedt, 2000a; Karato and Wu, 1993). The non-Newtonian viscosity structure does not have a substantial effect on the 2D corner-flow streamlines, relative to the Newtonian case, but results in the lowest viscosities in a two-lobed structure bounding the asthenospheric wedge where strain rates are the greatest (Fig. 3), which strongly influences the pressure-driven flow structure.

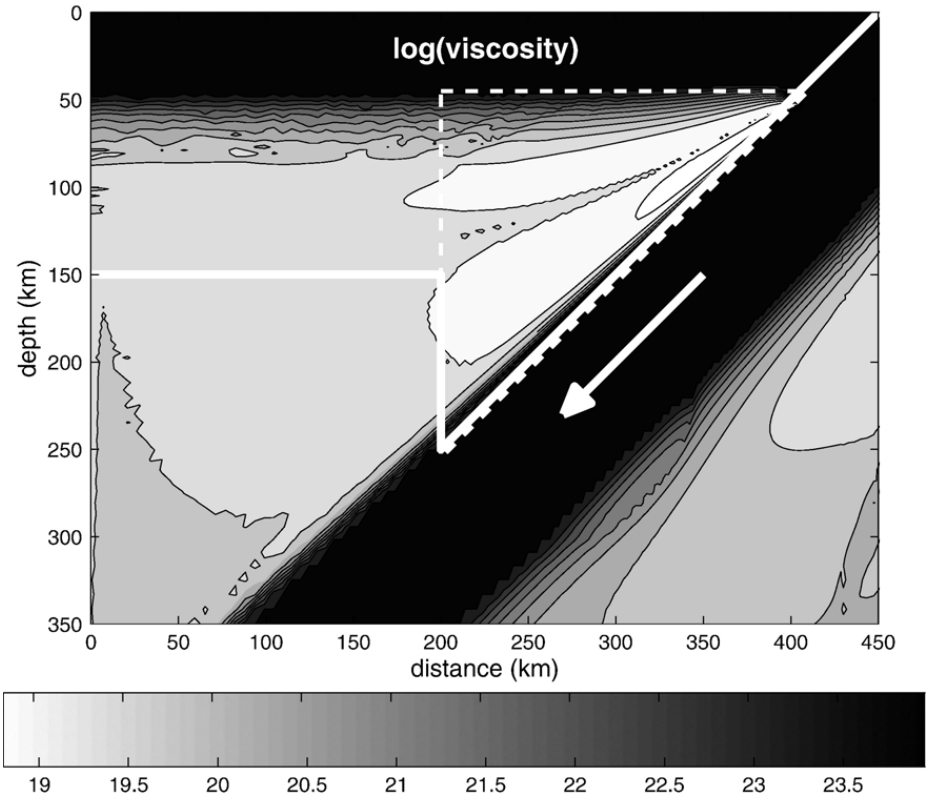

Fig. 3. Viscosity structure in log units of Pa·s determined by a 2D finite-element viscous flow model patterned after the Tonga slab. The non-Newtonian viscosity structure results in the lowest viscosities within a two-lobed structure bounding the asthenospheric wedge where strain rates are the greatest. Highest viscosities are in the slab and overlying plate. The dashed line delineates the region assumed to be a low-viscosity channel which is decreased by two log units to induce channelized flow within the arc asthenosphere. The solid white line separates the dislocation dominated regime (shallower) and diffusion dominated regime (deeper), with LPO development occurring in the dislocation regime. The dislocation regime is deeper beneath the arc than the backarc because of the higher strain rates at depth deepening the dislocation regime.

We calculate the along-strike flow pattern for a given viscosity structure and along-strike pressure gradient by numerically iterating to a solution for the equation,

$$\frac{\partial P}{\partial y} = \frac{\partial}{\partial x}\left(\eta \frac{\partial u_y}{\partial x}\right) + \frac{\partial}{\partial z}\left(\eta \frac{\partial u_y}{dz}\right), \quad (1)$$

where $\partial P/\partial y$ is the imposed pressure gradient, u_y is velocity in the along-strike (y) direction, and η is viscosity. The ratio of pressure gradient to the viscosity is more important than the exact magnitude of either value, so the induced flow rates may be adjusted nearly linearly by changes in either parameter. For simplicity, we keep the viscosity fixed at 10^{21} Pa s at 600 km depth for all cases and discuss the pressure gradient assuming that normalization. Pressure gradients on the order of a few kPa/km are sufficient to induce significant along-strike flow. For example, a sample case of $\partial P/\partial y$ equal to 10 kPa/km results in a peak trench-parallel velocity of 3–4 cm/yr at 180 km depth (Fig. 4a).

We track mineral texturing within the resultant flow field with D-Rex, a FORTRAN program which integrates progressive LPO development along streamlines within a given flow field (Kaminski et al., 2004) and has been successfully applied to a subduction setting (Lassak et al., 2006). We use an intermediate value of 125 for grain mobility, and a sub-grain nucleation parameter of five as described by Kaminski and Ribe (2001). These parameters are used only for calculations of LPO development and do not feed back into the rheology, which assumes a fixed grain size. Texturing begins with a number of randomly oriented mineral grains at the edges of the box which rotate with applied strain according to specified mineral slip systems (Kaminski and Ribe, 2001). For these models we assume the dominant deformation mechanism is dislocation creep, that the mantle is composed of 70% olivine and 30% enstatite, and that texturing only develops within the mantle wedge at depths shallower than 150 km in the backarc and 250 km beneath the arc as the stress dependent rheology likely deepens the dislocation creep regime in the upper wedge (Mei and Kohlstedt, 2000b; Pozgay et al., 2007). We do not consider any LPO development within the slab or overlying plate.

The local S splitting data across the basin come from a variety of back azimuths but the splitting parameters

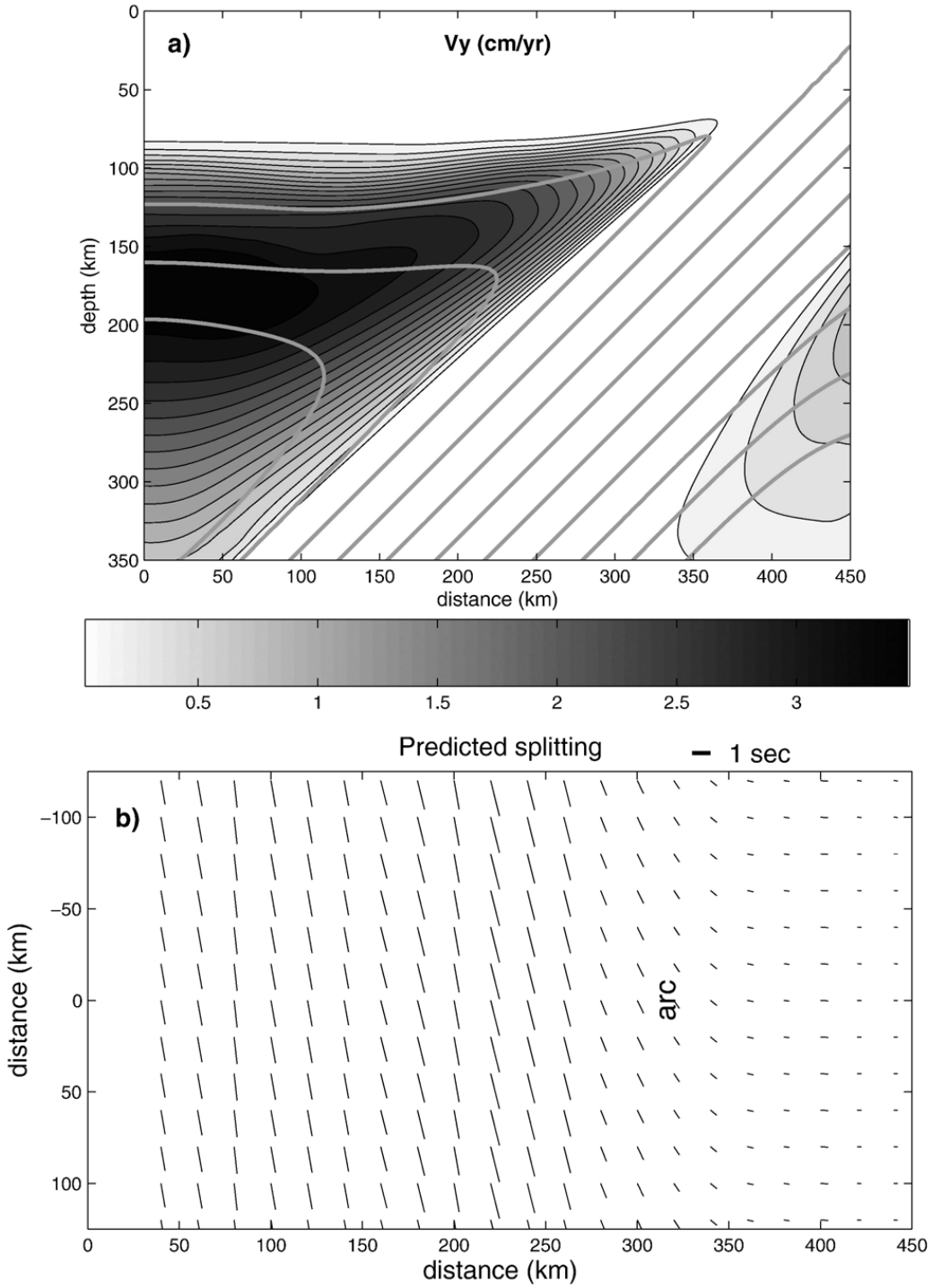

Fig. 4. a) Along-strike flow calculated for the viscosity structure shown in Fig. 2, with a cross dimensional pressure gradient of 10 kPa/km resulting in along-strike flow peaking at 3–4 cm/yr near 180 km depth in the backarc. Gray lines denote streamlines in 2D cross-sectional plane. b) Predicted fast S polarization at the surface for vertically traveling S waves through a model without a low-viscosity channel and a pressure gradient of 100 kPa/km (36 cm/yr peak velocity). This velocity is required to align the fast S polarization directions close to trench-parallel, but the largest rotations from convergence parallel occur in the backarc, contradictory to the observations. Map view shows pattern repeated along-strike to aid visualization.

remain relatively consistent at most individual stations (Smith et al., 2001) so for simplicity we compare our predictions with the stacked local S splitting results of Smith et al. The stacked results incorporate arrivals from a variety of backazimuths but with modest incidence angles due to limitations of the shear-wave window; these stacked results are well approximated by an "average" vertical raypath traveling from an earthquake in the slab immediately beneath the station. Each ray is evaluated piecewise for a fast orientation and split time

with the Christoffel equation, using the stiffness matrix of the locally-determined mineral texturing within the flow model. Evaluated raypath segments are smaller than the grid spacing of the model texturing, and binned into a histogram of fast S-wave polarization directions scaled to the accumulated splitting time for each fast axis orientation along the raypath (Fig. 5). The predicted splitting time of each raypath, δt, is a summation of the histogram given by

$$\delta t = \sum_{i=1}^{N} dt_i \cos(2\alpha), \tag{2}$$

where N is the number of bins in the histogram, dt_i is the split time accumulation of the ith bin, and α_i is the angle between the fast direction and the ith azimuth. The fast direction is given by the azimuth that results in the largest splitting time for the weighted summation — typically the peak of the histogram. This simplified weighted histogram approach breaks down for certain cases of anisotropic structure, notably the case of multiple layers with anisotropy of similar magnitude oriented ~45° apart (Silver and Savage, 1994), which requires more sophisticated waveform modeling including frequency effects to correctly evaluate the correct splitting parameters (Schulte-Pelkum and Blackman, 2003; Saltzer et al., 2000). However, the results are accurate for cases where the fast direction is relatively constant along the raypath or where the fast directions of individual layers are oriented roughly orthogonal to each other. Examination of the anisotropic orientation along the raypaths for our model demonstrates a predominant polarization orientation for nearly all of the rays (Fig. 5), validating this method for these particular models.

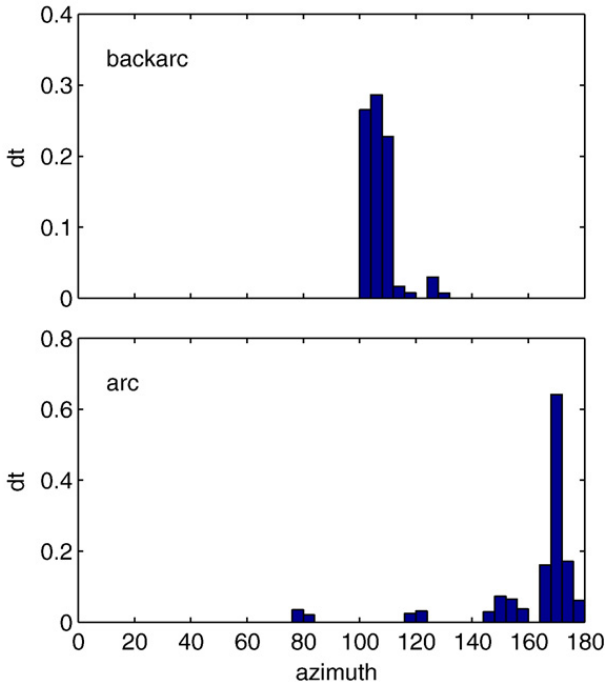

Fig. 5. Histograms showing splitting time accumulation for each orientation along a given raypath through the LPO model. Top panel is for a ray traveling beneath the backarc in our preferred model (Fig. 6) and has a clear peak at an azimuth of 104°, subparallel to the APM direction (90°). Bottom panel is for ray beneath the arc and has a clear peak at an azimuth of 166°, subparallel to the along-strike direction (180°).

3. Results

Increasing the applied along-strike pressure gradient in our models increases the along-strike flow rate and associated velocity gradients resulting in a rotation of a-axes from nearly trench- perpendicular everywhere for $\partial P/\partial y$ equal to zero to progressively more trench-parallel.

Splitting fast directions subparallel to the trench can be achieved in the above model with a high enough pressure gradient. However, with the assumed viscosity structure, the required pressure gradient is >100 kPa/km, greater than we infer from the dynamic topography. This may be accounted for by assuming a correspondingly lower overall mantle viscosity, but more problematically, the largest rotations occur beneath the backarc where the asthenospheric flow velocities are greatest (Fig. 4b, suggesting that a different viscosity structure is required to cause significant rotation in a-axes beneath the arc relative to the backarc.

A low-viscosity channel in the upper corner of the Lau mantle wedge a few hundred kilometers in lateral and depth extent is necessary to reconcile observed topography with the local geoid (Billen and Gurnis, 2001). Fluxing of the wedge with volatiles during slab dehydration can reduce the viscosity of the wedge considerably (Mei and Kohlstedt, 2000b; Hirth and Kohlstedt, 1996) and may be the cause of this low-viscosity channel. The dimensions of this channel are not tightly constrained, but must be on the order of a couple of hundred km in both lateral and depth extent. Such a channel helps reconcile the shear-wave splitting observations as well as the geoid and across-arc dynamic topography.

To examine the effects of a low-viscosity channel, we decrease the viscosity of the model in the upper wedge corner by two orders of magnitude (Fig. 3), using the dimensions of Billen and Gurnis (2001). We then apply a pressure gradient as before, inducing flow in the channel (Fig. 6). We match the splitting results persuasively well in both magnitude and direction using a pressure gradient of 8 kPa/km, resulting in fast directions subparallel to the convergence direction in the

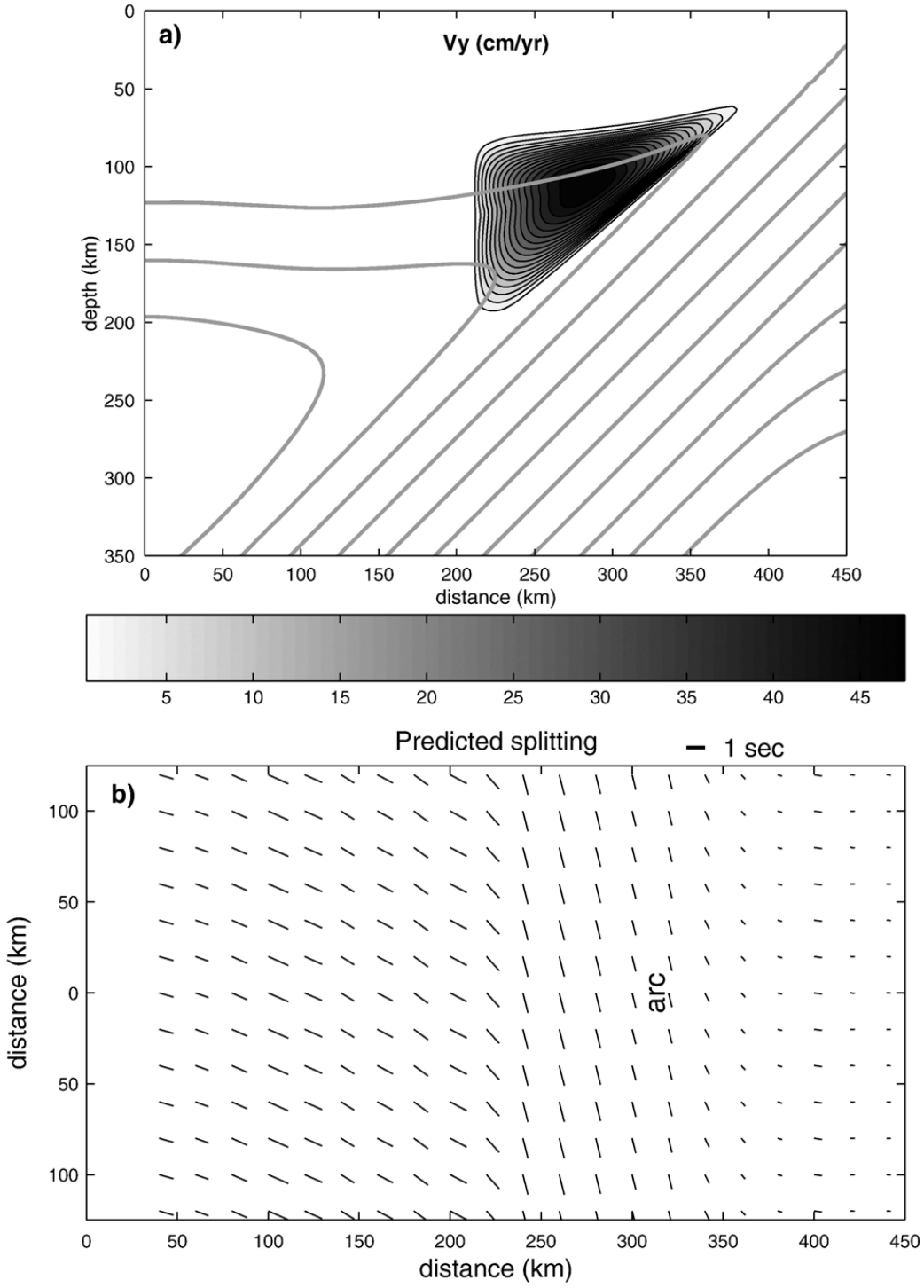

Fig. 6. a) Along-strike flow calculated for a model with a low-viscosity channel beneath the arc and a trench-parallel pressure gradient of 4 kPa/km. Along-strike flow is rapid, peaking at 48 cm/yr in the upper wedge. Gray lines denote streamlines in cross-sectional plane. b) Predicted fast directions at the surface for this low-viscosity channel model. The fast direction predictions are a good match to the observed fast directions with the largest rotations occurring beneath the arc and adjacent backarc. Further into the backarc, fast directions are parallel to the convergence direction. Predicted splitting times are about 1 s in the backarc, comparable to those observed (Fig. 1), and a few tenths of a second more than 1 s beneath the arc compared to a few tenths to nearly 2 s splitting in the observations.

backarc and nearly trench parallel beneath the arc (Fig. 6b). Predicted and observed splitting times in the backarc are both ~1 s. Observed splitting beneath the arc varies from a few tenths to nearly 2 s, while our predictions exhibit splitting times a few tenths of a second larger than 1 s beneath the arc.

4. Discussion

The velocity gradients necessary to reproduce the shear-wave splitting results require a peak velocity in the low-viscosity channel of roughly 48 cm/yr, nearly an order of magnitude faster than mantle motions are typically assumed to be. A degree of along-strike shearing less than that in the convergence direction will be unable to align the axes in trench-parallel orientation, but primarily affects the splitting times. In essence, to rotate the fast axes orthogonal to the convergence direction the along-strike strain rates must be much greater than the convergence direction strain rates which are enhanced by the relatively shallow dip of the Tonga slab. This requires a peak velocity in the low-viscosity channel 5–10 times the subducting plate velocity to account for the observed signal by strain induced mineral texturing. The observed small splitting times just to the east of the back-arc spreading center (Fig. 1) may indicate the presence of C-type fabrics in the wedge, which would exhibit similar splitting direction to our modeled A-type fabrics, but would have considerable smaller splitting times (Jung et al., 2006).

It is conceivable that the observed splitting signature is not primarily controlled by rapid, channelized mantle flow, but rather by the melt structure beneath the arc as aligned melt pockets or planes (Zimmerman et al., 1999; Mainprice, 1997). Seismic tomography suggests the presence of melt beneath the active arc to depths greater than 100 km (Conder and Wiens, 2006). Melt may affect the anisotropy structure in either of the two ways: alignment of high aspect ratio melt pockets (Schmeling, 1985) or melt segregation within a deforming matrix to form networks of weak zones, causing the olivine *a*-axes to rotate 90° from the shear direction (Holtzman et al., 2003). The first of these two mechanisms should exhibit a fast direction ~20° from the maximum extension direction (Zimmerman et al., 1999). An along-arc fast direction with this mechanism would require >30 cm/yr flow within the channel to rotate the axes ~60–70° with the melt still overprinting the mineral LPO seismic signature. The melt segregation mechanism tends to weaken the overall alignment (Holtzman et al., 2003), inconsistent with the splitting observations in the arc exhibiting some of the largest splitting times in the region (Fig. 1). Such a 90° rotation of *a*-axes relative to the extension direction for this mechanism also requires nearly zero along-axis flow, in conflict with the geochemical observations. Possibly most problematically, a melt induced anisotropy model would also have to explain why the fast directions rotate back to the absolute plate motion direction (APM) at the back-arc spreading center where there is also undoubtedly melt present. The effect of melt on the observed splitting warrants further investigation, but at present it is difficult to self-consistently satisfy the arc-parallel fast directions in the Lau basin with a primarily melt controlled model.

At least partially, the motivation for looking for alternative explanations for the shear-wave spitting pattern, such as melt effects, is aimed at getting around the idea of a rapidly flowing mantle. However, the 'speed limit' of the mantle is not constrained by observation, and our sense of 'reasonable mantle speed' relies heavily on geodynamic models, which in turn rely on suppositions of mantle viscosity and driving forces — often determined by plate speeds.

Assuming internal pressure gradients in the mantle of the order of a few tens of kPa/km coupled with the requirement of a low-viscosity channel beneath the Tonga arc (Billen and Gurnis, 2001), the asthenosphere will flow along-strike at a rate of ~50 cm/yr beneath the Tonga volcanic arc, self-consistently satisfying the geophysical and geochemical observations. The along-arc rate at Lau may be extreme relative to other subduction systems with along-arc flow signatures like Mariana (Pozgay et al., 2007) and South Sandwich (Leat et al., 2004) because of its unique geological environment with high rollback rates and free slab edge at the northern end and possible influence of the Samoan plume.

Acknowledgments

Thanks are due to Eduord Kaminski for making the D-Rex code available and for his openness to answering the questions regarding the program and mineral texturing. We also thank Peter Kelemen and Magali Billen for comments prior to submission. Thoughtful reviews by Donna Blackman and an anonymous reviewer greatly improved this manuscript. This work was supported by NSF grants OCE-0305292 and EAR-0649056.

References

Bevis, M., 1995. Geodetic observations of very rapid convergence and back-arc extension at the Tonga Arc. Nature (London) 374 (6519), 249–251.

Billen, M.I., Gurnis, M., 2001. A low viscosity wedge in subduction zones. Earth Planet. Sci. Lett. 193 (1–2), 227–236.

Buttles, J., Olson, P., 1998. A laboratory model of subduction zone anisotropy. Earth Planet. Sci. Lett. 164, 245–262.

Conder, J.A., 2005. A case for hot slab surface temperatures in numerical viscous flow models of subduction zones with an improved fault zone parameterization. Phys. Earth Planet. Inter. 149, 155–164.

Conder, J.A., Wiens, D.A., 2006. Seismic structure beneath the Tonga arc and Lau back-arc basin determined from joint Vp, Vp/Vs

tomography. Geochem. Geophys. Geosystems 7 (3), Q03018. doi:10.1029/2005GC001113.

Conder, J.A., Forsyth, D.W., Parmentier, E.M., 2002. Asthenospheric flow and asymmetry of the East Pacific Rise, MELT area. J. Geophys. Res. 107, 2344. doi:10.1029/2001JB000807.

Fischer, K.M., et al., 1998. Anisotropy and flow in Pacific subduction zone back-arcs. Pure Appl. Geophys. 151, 463–475.

Hall, C.E., et al., 2000. The influence of plate motions on three-dimensional back arc mantle flow and shear wave splitting. J. Geophys. Res. 105, 28,009–28,033.

Hirth, G., Kohlstedt, D.L., 1996. Water in the oceanic upper mantle: implications for rheology, melt extraction and the evolution of the lithosphere. Earth Planet. Sci. Lett. 144, 93–108.

Holtzman, B.K., et al., 2003. Melt segregation and strain partitioning: Implications for seismic anisotropy and mantle flow. Science 301, 1227–1230.

Honda, S., Yoshida, T., 2005. Effects of oblique subduction on the 3-D pattern of small-scale convection within the mantle wedge. Geophys. Res. Lett. 32 (13), 1–4.

Jung, H., Karato, S.-I., 2001. Water induced fabric transitions in olivine. Science 293, 1460–1463.

Jung, H., et al., 2006. Effect of water and stress on the lattice-preferred orientation of olivine. Tectonophysics 421 (1–2), 1–22.

Kaminski, E., Ribe, N.M., 2001. A kinematic model for recrystallization and texture development in olivine polycrystals. Earth Planet. Sci. Lett. 189 (3–4), 253–267.

Kaminski, E., Ribe, N.M., Browaeys, J.T., 2004. D-Rex, a program for calculation of seismic anisotropy due to crystal lattice preferred orientation in the convective upper mantle. Geophys. J. Int. 158 (2), 744–752.

Karato, S.-I., Wu, P., 1993. Rheology of the upper mantle: a synthesis. Science 260 (5109), 771–778.

Kneller, E.A., et al., 2005. B-type olivine fabric in the mantle wedge: insights from high-resolution non-Newtonian subduction zone models. Earth Planet. Sci. Lett. 237 (3–4), 781–797.

Lassak, T.M., et al., 2006. Seismic characterization of mantle flow in subduction systems: can we resolve a hydrated mantle wedge? Earth Planet. Sci. Lett. 243 (3–4), 632–649.

Leat, P.T., et al., 2004. Magma genesis and mantle flow at a subducting slab edge: the South Sandwich arc-basin system. Earth Planet. Sci. Lett. 227 (1–2), 17–35.

Mainprice, D., 1997. Modelling the anisotropic seismic properties of partially molten rocks found at mid-ocean ridges. Tectonophysics 279, 161–179.

Mehl, L., et al., 2003. Arc-parallel flow within the mantle wedge: evidence from the accreted Talkeetna arc, south central Alaska. J. Geophys. Res. 108, 2375. doi:10.1029/2002JB002233.

Mei, S., Kohlstedt, D.L., 2000a. Influence of water on plastic deformation of olivine aggregates 1. Diffusion creep regime. J. Geophys. Res. B: Solid Earth 105 (B9), 21457–21469.

Mei, S., Kohlstedt, D.L., 2000b. Influence of water on plastic deformation of olivine aggregates 2. Dislocation creep regime. J. Geophys. Res. B: Solid Earth 105 (9), 21,471–21,481.

Mizukami, T., Wallis, S.R., Yamamoto, J., 2004. Natural examples of olivine lattice preferred orientation patterns with a flow-normal *a*-axis maximum. Nature 427 (6973), 432–436.

Pearce, J.A., Stern, R.J., 2006. The origin of back-arc basin magmas: trace element and isotope perspectives. In: Christie, D.M. (Ed.), Back-Arc Spreading Systems — Geological, Biological, Chemical, and Physical Interactions. AGU Monograph.

Phipps, J., Smith, W.H.F., 1992. Flattening of the sea-floor depth–age curve as a response to asthenospheric flow. Nature 359 (6395), 524–527.

Pillet, R., et al., 1999. Crust and upper mantle heterogeneities in the southwest Pacific from surface wave phase velocity analysis. Phys. Earth Planet. Inter. 110 (3–4), 211–234.

Pozgay, S.H., Wiens, D.A., Conder, J.A., 2002. Complex mantle flow in the Mariana subduction system: evidence from shear wave splitting. Geophys. J. Int. 107, 371–388. doi:10.1111/j.1365-246X.2007.03433.x.

Saltzer, R.L., Gaherty, J.B., Jordan, T.H., 2000. How are vertical shear wave splitting measurements affected by variations in the orientation of azimuthal anisotropy with depth? Geophys. J. Int. 141 (2), 374–390.

Schmeling, H., 1985. Numerical models on the influence of partial melt on elastic, anelastic and electric properties of rocks; Part 1, Elasticity and anelasticity. Phys. Earth Planet. Inter. 41 (1), 34–57.

Schulte-Pelkum, V., Blackman, D.K., 2003. A synthesis of seismic P and S anisotropy. Geophys. J. Int. 154 (1), 166–178.

Silver, P.G., Savage, M.K., 1994. The interpretation of shear-wave splitting parameters in the presence of two anisotropic layers. Geophys. J. Int. 119 (3), 949–963.

Smith, G.P., et al., 2001. A complex pattern of mantle flow in the Lau backarc. Science 292, 713–716.

Taylor, B., et al., 1996. Sea-floor spreading in the Lau back-arc basin. Earth Planet. Sci. Lett. 144 (1–2), 35–40.

Turner, S., Hawkesworth, C., 1998. Using geochemistry to map mantle flow beneath the Lau Basin. Geology (Boulder) 26 (11), 1019–1022.

U.S. Department of Commerce, 2006. N.O.A.A., 2-minute Gridded Global Relief Data (ETOPO2v2). National Geophysical Data Center.

Yale, M.M., Phipps Morgan, J., 1998. Asthenosphere flow model of hotspot–ridge interactions; a comparison of Iceland and Kerguelen. Earth Planet. Sci. Lett. 161 (1–4), 45–56.

Zimmerman, M.E., et al., 1999. Melt distribution in mantle rocks deformed in shear. Geophys. Res. Lett. 26, 1505–1508.

Zhang, S., Karato, S.-I., 1995. Lattice preferred orientation of olivine aggregates deformed in simple shear. Nature 375, 774–777.